Towards the Reconstruction of Time-dependent Vibronic States from Nonlinear Wavepacket Interferometry Signals

Travis S. Humble and Jeffrey A. Cina*

Department of Chemistry and Oregon Center for Optics, University of Oregon, Eugene, OR 97403, USA
Received April 14, 2003

We present one-color nonlinear wavepacket interferometry (WPI) signal calculations for a system of two electronic levels and one vibrational degree of freedom. We consider two cases, a displaced harmonic oscillator system, which can be treated analytically, and a model photodissociative system, whose WPI signal must be calculated by numerical wavepacket propagation. We show how signals obtained with different combinations of intrapulse-pair phase shifts can be combined to isolate the complex-valued overlap between a given one-pulse target wavepacket and a variable three-pulse reference wavepacket. We demonstrate that with a range of inter- and intrapulse-pair delays the complex overlaps and variable reference states can be used to reconstruct the target wavepacket. We compare our results with previous methods for vibronic state reconstruction based on linear WPI and discuss further generalizations of our method.

Key Words : Ultrafast electronic spectroscopy, Coherent control of molecular dynamics, Wavepacket interferometry, State reconstruction

Introduction

Wavepacket interferometry signals differ from conventional (homodyne detected) ultrafast optical measurements because they are linear, rather than bilinear, in an excited-state wavepacket prepared by a given laser pulse. Linear[1] and nonlinear[2] WPI signals can be expressed in terms of the complex-valued overlap between the given one-pulse (target) wavepacket and a variable one- or three-pulse reference wavepacket, respectively. We have argued previously that the overlaps measured in a nonlinear WPI experiment can in some cases be used to exhaustively characterize the target wavepacket.[2] In this paper we show explicitly how this vibronic state reconstruction procedure can be carried out.

State reconstruction has been an objective in quantum physics for some time. Pioneering work by Vogel and Risken showed theoretically that the measurement of marginal probability distributions for the rotated quadrature phase can be inverted to determine a quasiprobability distribution function that is formally equivalent to the density matrix.[3] Smithey *et al.* implemented this technique by using balanced optical homodyne tomography to measure quadrature-field amplitudes for vacuum and squeezed states of the radiation field.[4] The data were then inverted to reconstruct the Wigner distribution function for a single mode of the radiation field.

Attempts at molecular state determination have been more recent. As a means of characterizing photoinduced dynamics, vibronic state determination for molecular systems could provide a useful diagnostic tool in coherent and/or optimal control experiments capable of identifying a shaped wavepacket created by an unknown waveform. In addition, under conditions where the driving pulses are well known, state determination has the potential to characterize dynamics on *unknown* excited-state potential energy surfaces by extracting nuclear amplitude level information from the measured signal.

Walmsley and coworkers used optical heterodyne tomography for the determination of vibrational wavepackets in diatomic molecules.[5] This form of emission tomography measures time- and frequency-resolved fluorescence but is restricted to diatomic molecules with nearly harmonic potentials. A method of "quantum state holography" was recently proposed to characterize vibrational wavepackets.[6] Using a pair of phase-locked pulses and measuring the time- and frequency-integrated fluorescence, quantum state holography is a form of linear WPI that could be used to reconstruct an object state from a set of complex overlaps with variable one-pulse reference wavepackets.

In this paper we further examine a recently proposed approach to state determination by *nonlinear* WPI,[2] an application of time-domain multi-dimensional electronic interference spectroscopy,[7-10] which has some features in common with earlier methods, but is much more flexible and more generally applicable. We begin by reviewing the theoretical background for the calculation of nonlinear WPI signals and show how combinations of signals obtained with different intrapulse-pair phase-locking angles can be used to isolate the complex-valued overlaps between a one-pulse target wavepacket and a large set of three-pulse reference wavepackets. Next we formulate a state reconstruction scheme based on singular value decomposition with back-substitution using the nonlinear WPI signal as input. To demonstrate nonlinear WPI, we derive an analytical expression for the signal in the case of the displaced harmonic oscillator model and numerically calculate the signal using wavepacket propagation techniques for the case of a model photodissociative system. Using the calculated WPI signal from the model photodissociative system we

*Corresponding Author. e-mail: cina@uoregon.edu

reconstruct the one-pulse target state using our state reconstruction procedure.

Theory

We consider a time-dependent Hamiltonian,

$$H(t) = H + V(t)\,, \tag{1}$$

composed of a time-independent molecular Hamiltonian H and a time-dependent external potential $V(t)$. For both two-electronic-level systems considered below, the molecular Hamiltonian is of the form

$$H = |g\rangle H_g \langle g| + |e\rangle H_e \langle e|\,, \tag{2}$$

where $|g\rangle$ and $|e\rangle$ are the ground and excited electronic states and H_α is the corresponding nuclear Hamiltonian with $\alpha = g, e$. The time-dependent external potential,

$$V(t) = -\sum_j \hat{\mu} \cdot \mathbf{E}_J(t); \quad J = A, B, C, D, \tag{3}$$

accounts for the interaction between the molecule and a sequence of four ultrashort laser pulses, where

$$\hat{\mu} = \boldsymbol{\mu}(|e\rangle\langle g| + |g\rangle\langle e|) \tag{4}$$

is the electronic dipole moment operator. The Jth electric field,

$$\mathbf{E}_J(t) = \mathbf{e}_J A_J(t - t_J)\cos[\Omega_J \cdot (t - t_J) + \Phi_J]\,, \tag{5}$$

has polarization vector $\mathbf{e}_J$, temporal envelope $A_J(t - t_J)$, carrier frequency Ω_J, and phase Φ_J.[11] We specify that the A and B pulses are phase-locked such that $\Phi_B - \Phi_A = \Omega_p t_p + \phi_p$ where Ω_p is the phase-locking frequency and ϕ_p is an experimentally controlled phase-locking angle.[1] Similarly for the C and D pulses, we require that $\Phi_D - \Phi_C = \Omega_d t_d + \phi_d$, with Ω_d the phase-locking frequency and ϕ_d the phase-locking angle. However, *inter*pulse-pair optical phase differences are not controlled, and may formally be regarded as taking a random value between 0 and 2π on any given laser shot.

The WPI signal is proportional to the interference population, *i.e.* the portion of the excited-state population that is *quadrilinear* in the incident electric fields.[12] The relevant contributions to the excited-state probability amplitude are therefore due either to the effects of a single pulse or a combination of three different pulses.[13] There are thus eight relevant contributions to the excited-state probability amplitude, each of which can be expressed through the action of an operator on the initial vibrational state, assumed here to be an eigenstate, $|n_g\rangle$, of H_g. The resulting excited-state probability amplitude (through third order in perturbation theory) at a time after the last pulse is[2,14]

$$\langle e|\Psi(t)\rangle = e^{-iH_e t}(U_A + U_B + U_C + U_D + T_A + T_B + T_C + T_D)|n_g\rangle\,. \tag{6}$$

The one-pulse U_J operators are

$$U_A = e^{-iH_e(t_p + t_w + t_d)} P_A e^{iH_g(t_p + t_w + t_d)} \tag{7a}$$

$$U_B = e^{-iH_e(t_w + t_d)} P_B e^{iH_g(t_w + t_d)} \tag{7b}$$

$$U_C = e^{-iH_e t_d} P_C e^{iH_g t_d} \tag{7c}$$

$$U_D = P_D\,, \tag{7d}$$

while the three-pulse T_J operators are

$$T_A = -P_D e^{-iH_g t_d} P_C^\dagger e^{-iH_e t_w} P_B e^{iH_g(t_w + t_d)} \tag{8a}$$

$$T_B = -P_D e^{-iH_g t_d} P_C^\dagger e^{-iH_e(t_p + t_w)} P_A e^{iH_g(t_p + t_w + t_d)} \tag{8b}$$

$$T_C = -P_D e^{-iH_g(t_w + t_d)} P_B^\dagger e^{-iH_e t_p} P_A e^{iH_g(t_p + t_w + t_d)} \tag{8c}$$

$$T_D = -e^{-iH_e t_d} P_C e^{iH_g t_w} P_B^\dagger e^{-iH_e t_p} P_A e^{iH_g(t_p + t_w + t_d)}\,. \tag{8d}$$

The operator P_J, referred to as the Jth pulse propagator, specifies the effects of the Jth pulse on the vibrational wavepackets during $|e\rangle \leftarrow |g\rangle$ electronic transitions. The Hermitian conjugate, $P_J^\dagger$, accounts for the same effects during $|g\rangle \leftarrow |e\rangle$ electronic transitions. Under the rotating wave approximation and neglecting the effects of pulse overlap,[15] the pulse propagator takes the form[16]

$$P_J = \frac{i\mu}{2} e^{-i\Phi_J} \int_{-\infty}^{\infty} d\tau A_J(\tau) e^{iH_e \tau} e^{-i(H_g + \Omega_J)\tau}\,. \tag{9}$$

The U_J operators in Eqs. (7) act on the initial vibrational state by back-propagating the initial time-zero state $|n_g\rangle$ to the arrival time of the Jth pulse and then transferring nuclear amplitude from the ground to excited surface *via* P_J. This transferred wavepacket then evolves under the excited-state Hamiltonian until time 0. Each wavepacket created by a U_J operator is proportional to the Jth electric field.[17]

The effects of the T_J operators in Eqs. (8) on the initial vibrational state have a similar interpretation. After back-propagation, a pulse propagator transfers amplitude from the ground state to the excited state where the wavepacket propagates until a second pulse propagator transfers the amplitude back to the ground state. Here the wavepacket evolves until a third pulse re-excites it to the excited surface where it propagates until time 0. The resulting wavepacket is trilinear in the contributing electric fields.[17]

The interference population calculated from the probability amplitude (6) has four contributing terms:

$$S = 2\mathrm{Re}\langle n_g|(T_A^\dagger U_A + T_B^\dagger U_B + T_C^\dagger U_C + T_D^\dagger U_D)|n_g\rangle\,. \tag{10}$$

Each U_J operator in Eq. (10) is matched with the corresponding T_J operator. By defining the complex quantity

$$J_0 = \langle n_g|T_J^\dagger U_J|n_g\rangle\big|_{(\phi_p,\phi_d)=(0,0)} \tag{11}$$

as the overlap between the states $U_J|n_g\rangle$ and $T_J|n_g\rangle$ with both phase-locking angles set to zero, the WPI signal can be re-expressed as

$$S(\phi_p,\phi_d) = 2\mathrm{Re}[(A_0 + D_0^*)e^{i(\phi_p+\phi_d)} + (B_0 + C_0)e^{i(\phi_d-\phi_p)}]. \tag{12}$$

The presence of terms involving the sum and difference of the experimentally controlled phase-locking angles suggests a phase-cycling scheme in which signals collected at different (ϕ_p,ϕ_d) are combined to isolate the $A_0 + D_0^*$ and $B_0 + C_0$ overlaps. As discussed below, the ability to isolate these contributions to the signal will prove useful for reconstructing the target vibronic state $U_C|n_g\rangle$ from nonlinear WPI data. In particular, our interest will be in the real and imaginary parts of the $B_0 + C_0$ overlaps, which can be isolated as

$$\mathrm{Re}[B_0 + C_0] = \frac{1}{4}\left[S(0,0) - S\left(-\frac{\pi}{2},\frac{\pi}{2}\right)\right] \tag{13a}$$

$$\mathrm{Im}[B_0 + C_0] = \frac{1}{4}\left[S\left(-\frac{\pi}{2},0\right) - S\left(0,-\frac{\pi}{2}\right)\right]. \tag{13b}$$

State Reconstruction

As shown in Eqs. (13), the sum of B_0 and C_0 overlaps is isolable from the total signal by combining signals obtained with different combinations of phase-locking angles.[1,18] In cases where the B_0 contribution is temporally well separated from the C_0 contribution or is negligible (as will be the case for the model dissociative system discussed below, but not for a one-dimensional displaced harmonic oscillator) it becomes possible to completely isolate the C_0 overlap. The collection of C_0 values for various t_p and t_w corresponds to the overlap of a one-pulse target state created by the U_C operator with various three-pulse reference states determined by the T_C operator. As noted previously,[2] when considering the case of displaced uncoupled harmonic potentials and transform limited pulses with durations less than the inverse absorption bandwidth, the reference states belong to a family of coherent states. When the collection of overlaps between the target and reference states is effectively exhaustive, the C_0 contribution comprises a full set of expansion coefficients for the target state in a coherent state representation. Knowledge of the coherent basis states would then allow the reconstruction of the target state using the experimentally determined expansion coefficients. We now further develop the idea of state reconstruction using a more general scheme suited to arbitrary potentials.

When C_0 is isolable, we can rewrite the entire collection of delay dependent overlaps as

$$\mathbf{A_{Ref}x_{Tar}} = \mathbf{b_{Sig}}. \tag{14}$$

For a collection of M pairs of time delays (t_p, t_w) and an N-point spatial grid for the wavefunction expansion,[19] the reference matrix $\mathbf{A_{Ref}}$ is a real 2M-by-2N matrix partitioned into four submatrices as

$$\mathbf{A_{Ref}} = \begin{pmatrix} \mathbf{A_r} & -\mathbf{A_i} \\ \mathbf{A_i} & \mathbf{A_r} \end{pmatrix}. \tag{15}$$

$\mathbf{A_r}$ is a real M-by-N matrix whose elements are $\mathrm{Re}\langle n_g|T_C^\dagger|x_n\rangle$, and $\mathbf{A_i}$ is a real M-by-N matrix whose elements are $\mathrm{Im}\langle n_g|T_C^\dagger|x_n\rangle$. The 2$N$-by-*1* vector $\mathbf{x_{Tar}}$ is the target wavefunction partitioned so that the first N elements are $\mathrm{Re}\langle x_n|U_C|n_g\rangle$ and the second N elements are $\mathrm{Im}\langle x_n|U_C|n_g\rangle$. The vector $\mathbf{b_{Sig}}$ is a real *2M*-by-*1* vector whose first M elements contain the real components of C_0 over the collection of time delays and whose second M elements contain the imaginary components of C_0.

Knowledge of the signal $\mathbf{b_{Sig}}$ and the reference matrix $\mathbf{A_{Ref}}$ can be used to obtain a solution to Eq. (14) in the least squares sense using singular value decomposition (SVD**)**. The SVD of the 2M-by-2N matrix $\mathbf{A_{Ref}}$ is[20]

$$\mathbf{A_{Ref}} = \mathbf{UWV^T}, \tag{16}$$

where $\mathbf{U}$ is a 2M-by-2N row-orthogonal matrix, $\mathbf{W}$ is a diagonal 2N-by-2N matrix with elements $(\mathbf{W})_{ij} \geq 0$, and $\mathbf{V}$ is a 2N-by-2N orthogonal matrix. Using the SVD of $\mathbf{A_{Ref}}$ and backsubstitution of the signal $\mathbf{b_{Sig}}$ one finds the vector $\mathbf{x_{SVD}}$**,** which minimizes the norm, $|\mathbf{x_{SVD}}|$, and the residual, $|\mathbf{A_{Ref}x_{SVD} - b_{Sig}}|$, according to

$$\mathbf{x_{SVD}} = \mathbf{VW_M^{-1}U^Tb_{Sig}}, \tag{17}$$

The matrix $\mathbf{W_M}$ is the matrix $\mathbf{W}$ modified by setting to *infinity* those diagonal elements that are 0. $\mathbf{W_M^{-1}}$ is the inverse of $\mathbf{W_M}$. In the case that $\mathbf{W}$ has only nonzero diagonal elements, then $\mathbf{x_{SVD}}$ is the exact solution to Eq. (14).

Signal Calculations

As an example of a nonlinear WPI signal we first consider a system of two electronic levels supporting one-dimensional harmonic oscillator potentials whose minima are displaced from one another by a distance d. For this system it is possible to obtain analytical expressions for the eight operators in Eqs. (7) and (8) and for the signal in Eq. (10) for the case of transform limited pulses whose durations are much smaller than the inverse frequency-width of the absorption spectrum. We choose $n_g = 0$ and utilize the properties of the harmonic oscillator coherent states.[21] In particular, the generalized translation operator $D(\alpha) = \exp(\alpha a^\dagger - \alpha^* a)$, where a and $a^\dagger$ are the lowering and raising operators**,** is used to shift the excited-state Hamiltonian by the dimensionless distance $\alpha_0 = (m\omega/2)^{1/2}d$, so that $H_e = D(\alpha_0)(H_g + \varepsilon)D^\dagger(\alpha_0)$, where ε is the bare electronic energy. Some straightforward manipulations lead to the following signal contributions (11).

$$\begin{aligned} A_0^{SHO} &= f\exp[i((\Omega_d - \varepsilon)t_d + (\Omega_p - \varepsilon)t_p)] \\ &\times \exp[\alpha_0^2(e^{-i\omega t_p} + e^{i\omega t_w} + e^{i\omega t_d} + e^{-i\omega(t_p + t_w + t_d)} \\ &- e^{-i\omega(t_p + t_w)} - e^{i\omega(t_w + t_d)} - 2)] \end{aligned} \tag{18a}$$

$$B_0^{SHO} = f\exp[i((\Omega_d - \varepsilon)t_d - (\Omega_p - \varepsilon)t_p)] \times \exp[\alpha_0^2(e^{i\omega t_p} - e^{-i\omega t_w} + e^{i\omega t_d} - e^{i\omega(t_p + t_w + t_d)} + e^{i\omega(t_p + t_w)} + e^{-i\omega(t_w + t_d)} - 2)] \quad (18b)$$

$$C_0^{SHO} = f\exp[i((\Omega_d - \varepsilon)t_d - (\Omega_p - \varepsilon)t_p)] \exp[\alpha_0^2(e^{i\omega t_p} - e^{i\omega t_w} + e^{-i\omega t_d} - e^{i\omega(t_p + t_w + t_d)} + e^{i\omega(t_p + t_w)} + e^{i\omega(t_w + t_d)} - 2)] \quad (18c)$$

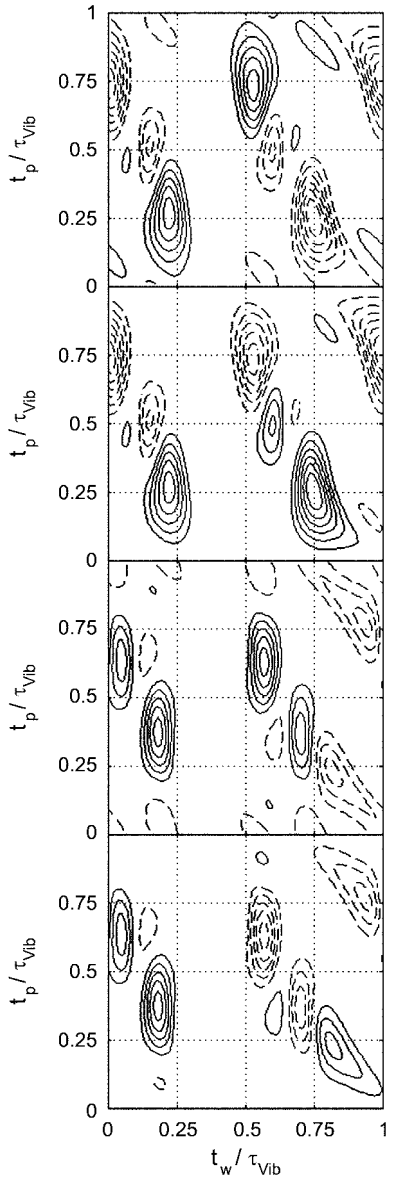

Figure 1. Plots of nonlinear WPI signals for a displaced harmonic oscillator model at four different phase-locking combinations: From top to bottom (ϕ_p, ϕ_d) = (0, 0), ($-\pi/2$, $\pi/2$), (0, $-\pi/2$), and ($-\pi/2$, 0). Solid (Dashed) lines are positive (negative) contours of dimensionless signal given by Eq. (10) divided by $|f|$ and have a maximum (minimum) value of 4 (–4) and a spacing of 4/7.

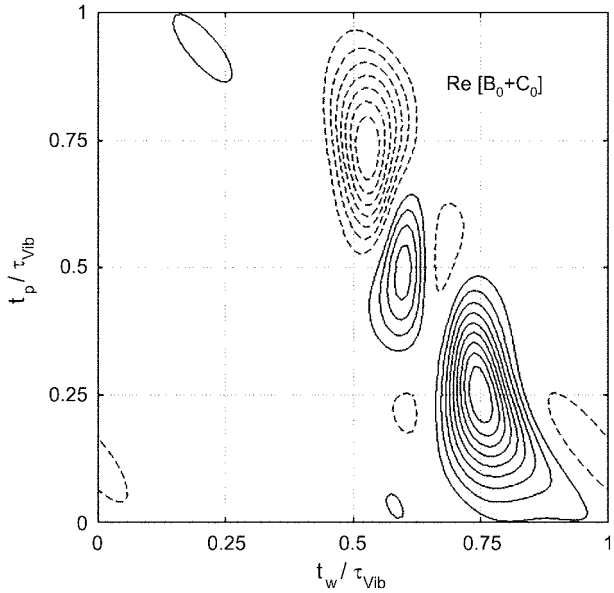

Figure 2. The real part of $B_0^{SHO} + C_0^{SHO}$ obtained by combining WPI signals according to Eq. (13a) divided by $|f|$. Solid (Dashed) lines are positive (negative) contours with a maximum (minimum) value of 2 (–2) and a spacing of 2/7.

$$D_0^{SHO} = f\exp[-i((\Omega_d - \varepsilon)t_d + (\Omega_p - \varepsilon)t_p)] \exp[\alpha_0^2(e^{i\omega t_p} + e^{i\omega t_w} + e^{i\omega t_d} + e^{i\omega(t_p + t_w + t_d)} - e^{i\omega(t_p + t_w)} - e^{i\omega(t_w + t_d)} - 2)] \quad (18d)$$

where $f = -a_A a_B a_C a_D$ is a dimensionless prefactor, and $a_J = (\mu/2)\int_{-\infty}^{\infty} d\tau A_J(\tau)$.

The four contributions in Eq. (18) are used to calculate interferograms according to Eq. (12) for a system with m = 63.5 amu, $\omega = 2\pi c(250\ \text{cm}^{-1})$, and d = 0.09216 Å (α_0^2 = 1.9995). We fix the third time delay at $t_d = 0.25\tau_{\text{Vib}}$ = 33.35 fs, and set the carrier and phase-locking frequencies for both pulse-pairs equal to $\Omega_J = \Omega_{p,d} = \varepsilon + \alpha_0^2\omega$ (*i.e.* the vertical resonance frequency). The WPI signal is shown in Figure 1 under four phase-locking conditions sufficient to isolate the $B_0^{SHO} + C_0^{SHO}$ (or $A_0^{SHO} + D_0^{SHO*}$) contributions to the total signal. The real part of $B_0^{SHO} + C_0^{SHO}$, given by Eq. (13a), is shown in Figure 2 as an illustration of a quantity that can be isolated by phase-cycling.

In the two-level displaced harmonic oscillator model, straightforward dynamical separation of the B_0^{SHO} contribution from the C_0^{SHO} contribution is impossible; according to Eqs. (18b) and (18c) the real part of the exponent in each contribution is the same, whereas the imaginary part is not. The B_0^{SHO} and C_0^{SHO} contributions therefore have identical magnitudes but different phases at any (t_p, t_w). An analogous situation is found for A_0^{SHO} and D_0^{SHO*} in Eqs. (18a) and (18d). To rationalize these coincident magnitudes, Figure 3 shows classical phase-space diagrams for the trajectories of the $U_J|n_g\rangle$ and $T_J|n_g\rangle$ coherent states. We choose time delays that lead to maximal magnitude for both B_0^{SHO} and C_0^{SHO} (or A_0^{SHO} and D_0^{SHO*}) contributions. The diagrams

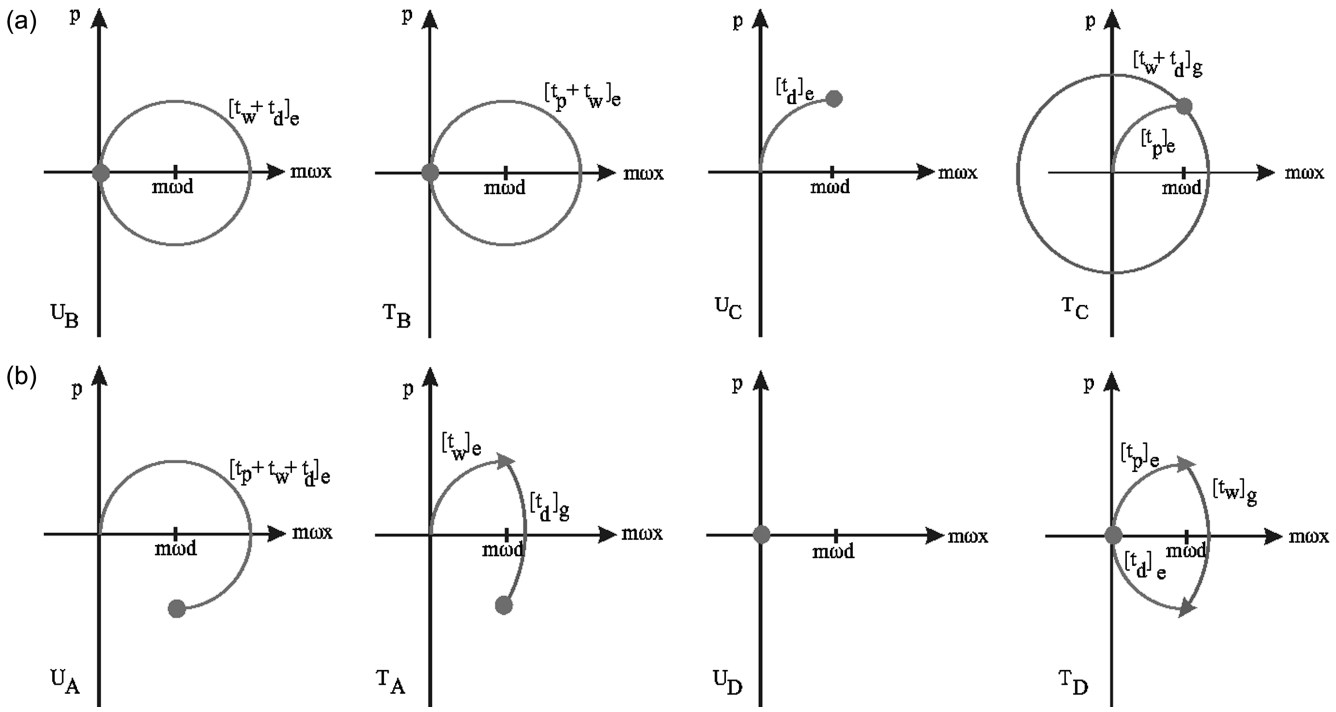

Figure 3. Phase-space diagrams for the $U_J|0\rangle$ and $T_J|0\rangle$ coherent states in the displaced harmonic oscillator system shown at a time delay that maximizes the J_0 contribution. The notation $[t]_\alpha$ implies time-evolution for time t under H_α. In (a) trajectories are shown, with $t_p = t_d = \tau_{\text{Vib}}/4$ and $t_w = 3\tau_{\text{Vib}}/4$, that lead to maxima in both C_0 and B_0 contributions. In (b) trajectories are shown, with $t_p = t_w = t_d = \tau_{\text{Vib}}/4$, that lead to maxima in both A_0 and D_0 contributions.

indicate that although the wavepacket dynamics are different for B_0^{SHO} and C_0^{SHO} (or A_0^{SHO} and D_0^{SHO*}) the overlap between the corresponding $U_J|n_g\rangle$ and $T_J|n_g\rangle$ states should be maximal for each term.

As a second case, we consider a two-level system with one vibrational degree of freedom in which wavepacket dynamics leads to a negligible B_0 contribution, *i.e.* a completely isolable C_0 contribution: a system with a harmonic ground state and an unbound excited state. Within the U_B and T_B operators given by Eqs. (7b) and (8b), respectively, wavepacket propagation during the t_w interval is on the excited-state potential. In the case of an unbound excited state and long t_w, the wavepackets associated with the U_B and T_B operators move well away from the Franck-Condon point by the time the third pulse arrives. Under these conditions, the B_0 contribution should be negligible as the wavepackets associated with the U_B and T_B operators will be disparate, as sketched in the phase-space diagram in Figure 4. Although our calculations here use vibrationally abrupt pulses, in any real experiment the B_0 contribution will be further diminished by spectral discrimination, as the T_B wavepacket will be outside the spatial region where the third laser pulse effectively transfers amplitude (illustrated by the blocked region in Fig. 4). Similar arguments can be made for the A_0 contribution. Long t_w does not diminish the C_0 contribution, because the wavepacket created by the T_C operator undergoes harmonic motion on the ground state during the t_w interval, while the wavepacket associated with U_C does not depend on t_w. Therefore the C_0 contribution repeats as a function of t_w with period τ_{Vib}. An analogous situation occurs for the overlap between the U_D and T_D wavepackets.[22]

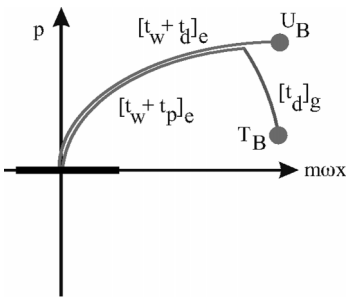

Figure 4. A schematic phase-space diagram for the case of a harmonic ground state and an unbound excited state using the time-dependent expectation values of position and momentum of $U_B|0\rangle$ and $T_B|0\rangle$ to demonstrate the effect of a long t_w delay on the B_0 contribution for fixed t_p and t_d. The notation $[t]_\alpha$ implies time-evolution for time t under H_α. The block region represents the resonant spatial range within which finite-bandwidth pulses would efficiently transfer amplitude between ground and excited states.

To make quantitative calculations on a photodissociative model, we consider a system with a harmonic ground state (using the same parameters as for the harmonic oscillator model) and an excited-state potential given by

$$V_e(x) = D_e e^{-\beta_e x} + \varepsilon' . \tag{19}$$

Our parameters are chosen so that the zeroth, first, and second derivatives of the potential (19) at the Franck-Condon point match the corresponding derivatives of the displaced harmonic oscillator excited-state potential previously

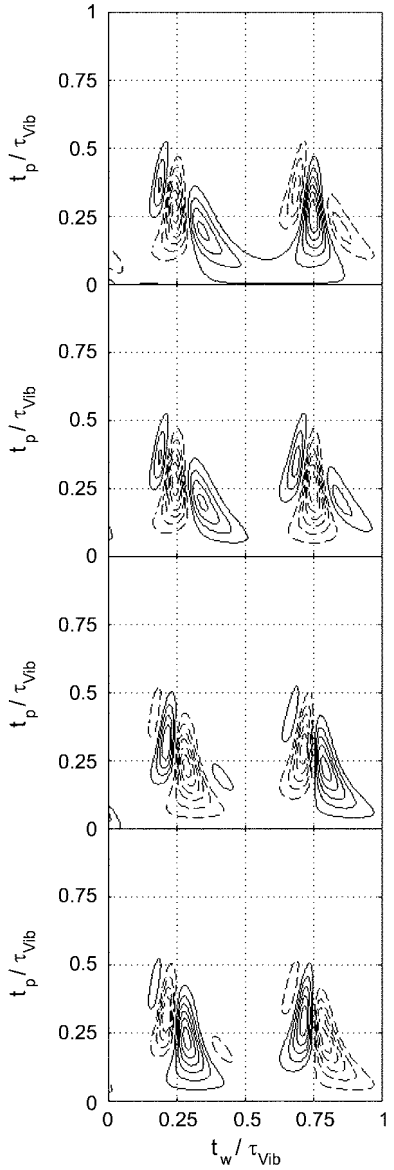

Figure 5. Calculated WPI signals at four different phase-locking combinations for the dissociative system. From top to bottom: (ϕ_p, ϕ_d) = (0, 0), ($-\pi/2$, $\pi/2$), (0, $-\pi/2$), and ($-\pi/2$, 0). Solid (Dashed) lines are positive (negative) contours of dimensionless signal given by Eq. (10) divided by $|f|$ and have a maximum (minimum) value of 2 (–2) and a spacing of 2/7.

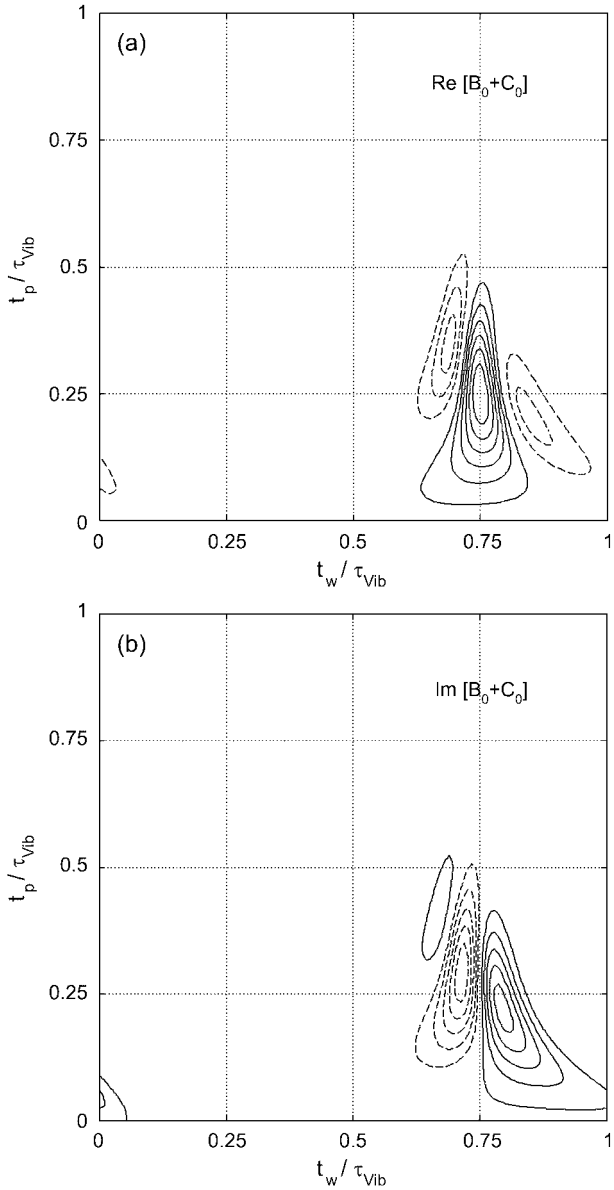

Figure 6. The (a) real and (b) imaginary components of the C_0 contribution for the dissociative system divided by $|f|$. The components are obtained by combining signals with different optical phase shifts according to Eq. (13). Notice that the B_0 contribution is barely visible, at small t_w and t_p. Solid (Dashed) lines are positive (negative) contours of dimensionless signal and have a maximum (minimum) value of 1 (−1) and a spacing of 1/7.

discussed. This allows for a consistency check between our calculated signal and the harmonic oscillator system, as the excited-state dynamics should be similar for short times. To satisfy these conditions we use a bare electronic difference energy $\varepsilon' = \varepsilon - 2\omega$, a Franck-Condon energy $D_e = 2\pi c$ (1000 cm^{-1}) and an inverse length scale $\beta_e = 10.85$ Å^{-1}. The excited-state probability amplitude (6) for this system was calculated by wavepacket propagation on a spatial grid using the split-operator technique[23] with a time step of 0.01 fs.[24] In Figure 5 we show the resulting interferograms under four phase-locking conditions. These signals can be used to isolate the real and imaginary parts of $B_0 + C_0$, shown in Figs. 6(a) and 6(b), respectively.

As anticipated from our discussion of the wavepacket dynamics, the A_0 and B_0 contributions to the signal become negligible very quickly in the model photodissociative system, as these contributions decay to zero in less than $\tau_{Vib}/4$ in either the t_p or t_w directions. As a result the isolated contributions in Figures 6(a) and 6(b) are almost exclusively C_0. Although it is not shown here, the D_0^* contribution is similarly isolable as the sole significant contributor to $A_0 + D_0^*$. The C_0 and D_0^* contributions for the displaced harmonic oscillator and model photodissociative systems are similar in form for small t_p, though this is not visible from Figures 1 and 5 since the overlapping B_0 contribution is also

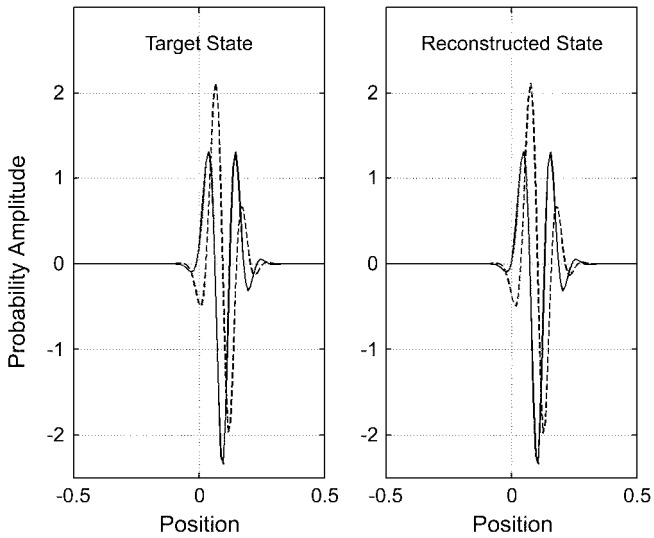

Figure 7. The target state (a) and the reconstructed state (b) obtained by singular value decomposition in the position representation from the signal in Fig. 6. Distance is measured in angstroms and probability amplitude has been divided by the dimensionless prefactor a_C.

present in the former case. For larger t_p, however, both C_0 and D_0^* contributions to the photodissociative system signal decay completely, which is in contrast to the periodic repetition of the same terms for the displaced harmonic oscillator. The location of peak C_0 magnitude for the photodissociative system can be predicted by determining when the reference state maximally overlaps the target state. Using classical trajectory arguments the magnitude is expected to occur at ($t_p = t_d$, $t_w = \tau_{\text{Vib}} - t_d$) as this reference wavepacket most closely coincides with the target wavepacket in phase-space. For times $t_p > t_d$ the signal magnitude is expected to decay permanently as observed in Figure 6 because the reference wavepackets become more distant from the target state.

For state reconstruction we use the isolable C_0 contribution from the model photodissociative system as $\mathbf{b_{Sig}}$ and construct the reference matrix $\mathbf{A_{Ref}}$ using the numerically propagated reference wavepackets. We use 50 equally spaced values for both the t_p and t_w delay parameters, ranging from 0 fs to τ_{Vib} = 133.4 fs.[25] We use the SVD routine from Reference 20 to calculate Eq. (16) and make use of the resulting **U**, **W**, and **V** matrices to reconstruct the 512-by-1 vector $\mathbf{x_{SVD}}$ according to Eq. (17).[26] The magnitude of the overlap between the numerically propagated target state, shown in Figure 7(a), and the reconstructed state, shown in Figure 7(b), was unity within machine precision.

Discussion and Concluding Remarks

We have presented calculations of nonlinear WPI signals for a displaced harmonic oscillator system and a model photodissociative system. We have shown that the complex-valued overlap between a target wavepacket and a variable reference wavepacket can be experimentally determined by combining signals with different phase-locking angles.[27] For the case of the model photodissociative system, we demonstrated how the measurement of a set of overlaps between a given one-pulse target state and variable three-pulse reference states can be used to accurately reconstruct the target wavepacket.

Averbukh *et al.*[6] recently put forward a related method for vibronic state reconstruction termed quantum state holography. In quantum state holography a single pair of pulses prepares both a target state and a reference state on an excited-state potential. Measurements of the time- and frequency-integrated fluorescence under different phase-locking conditions and for variable intrapulse-pair delay provide the overlap between a one-pulse target state and a set of variable one-pulse reference states. Signal measurements and prior knowledge of the energy eigenstates of the excited-state potential lead to a set of simultaneous equations that can be inverted using an SVD procedure similar to the one employed in this paper. Averbukh *et al.* also considered an alternative reconstruction method based on coherence observation by interference noise. The latter approach, however, relies on a signal that is bilinear rather than linear in the target wavepacket.

From the perspective of the present paper, quantum state holography[6] is a form of linear WPI. The variable one-pulse reference states prepared in a linear WPI experiment are restricted to a one-dimensional subspace of the system's phase space parametrized by the intrapulse-pair delay. Isolation of the complex overlap between one-pulse target and reference states in linear WPI by phase-cycling was demonstrated in the second paper of Reference 1. In nonlinear WPI reference states are prepared by a sequence of three pulses and are not restricted to a one-dimensional subspace. Greater exploration of the system's Hilbert space with the three-pulse reference wavepackets in nonlinear WPI provides a greatly expanded set of overlaps between the target and reference states and therefore allows more thorough characterization of the target state. As is evident from the reconstruction of a squeezed-state wavepacket in Reference 6, the restriction of linear WPI reference states to the Franck-Condon energy shell limits the collection of overlaps between the target and reference states and can diminish the fidelity of the reconstruction. The determination of a target state prepared by a shaped pulse may therefore be incomplete in a linear WPI experiment.[28]

An additional advantage afforded by nonlinear WPI is the possibility of performing two-color measurements, in which the A and B pulses would drive transitions between the ground electronic state and an intermediate electronic state, while the C and D pulses drive transitions between the ground state and a final (perhaps higher-lying) electronic state. In this scenario the A_0 and B_0 contributions to the signal are negligible because the A and B pulses are not resonant with the ground-state-to-final-state transition. The reference matrix of Eq. (14) will be well defined if the reference wavepackets are prepared on well-characterized ground and intermediate electronic states. Two-color nonlinear

WPI therefore would provide a means to probe the dynamics of a target wavepacket on an *unknown* higher-lying potential energy surface.

A possible extension of nonlinear WPI as a state determination technique is to the reconstruction of a one-pulse excited-state *density matrix* increment prepared from a thermal ground state distribution. Our current efforts are focused on this topic as well as on incorporating the effects of finite duration pulses into our calculations using the pulse propagators defined in Eq. (9). We further intend to explore the inclusion of rotational states and additional vibrational degrees of freedom in nonlinear wavepacket interferometry signals.

Acknowledgments. This research was supported by a grant from the US National Science Foundation.

References

1. Scherer, N. F.; Carlson, R. J.; Matro, A.; Du, M.; Ruggiero, J.; Romero-Rochin, V.; Cina, J. A.; Fleming, G. R.; Rice, S. A. *J. Chem. Phys.* **1991**, *95*, 1487. Scherer, N. F.; Matro, A.; Ziegler, L. D.; Du, M.; Carlson, R. J.; Cina, J. A.; Fleming, G. R. *ibid.* **1992**, *96*, 4180.
2. Cina, J. A. *J. Chem. Phys.* **2000**, *113*, 9488.
3. Vogel, K.; Risken, H. *Phys. Rev. A* **1989**, *40*, 2847.
4. Smithey, D. T.; Beck, M.; Raymer, M. G.; Faridani, A. *Phys. Rev. Lett.* **1993**, *70*, 1244.
5. Dunn, T. J.; Walmsley, I. A.; Mukamel, S. *Phys. Rev. Lett.* **1995**, *74*, 884.
6. Averbukh, I. Sh.; Shapiro, M.; Leichtle, C.; Schleich, W. P. *Phys. Rev. A* **1999**, *59*, 2163.
7. Cho, M.; Scherer, N. F.; Fleming, G. F.; Mukamel, S. *J. Chem. Phys.* **1992**, *96*, 5618.
8. Cina, J. A.; Harris, R. A. *J. Chem. Phys.* **1994**, *100*, 2531.
9. de Boeij, W. P.; Pshenichnikov, M. S.; Wiersma, D. A. *Chem. Phys.* **1998**, *233*, 287.
10. Hybl, J. D.; Albrecht Ferro, A.; Jonas, D. M. *J. Chem. Phys.* **2001**, *115*, 6606.
11. The relative time delays between electric fields are defined as: $t_p = t_B - t_A$, $t_w = t_C - t_B$, and $t_d = t_D - t_C$, with the arbitrary choice of $t_D = 0$. We only consider the case $t_A < t_B < t_C < t_D$, but other alternatives are possible. For simplicity, the electric field polarizations and dipole moment are taken to be parallel.
12. The excited-state interference population can be detected by measuring the time- and frequency-integrated fluorescence. The quadralinear contribution to the population can be isolated from the total fluorescence by separately detecting and subtracting signal contributions arising from one-, two-, and three-pulse induced fluorescence. See Reference 1.
13. Even combinations of pulses contribute to the ground state probability amplitude and higher odd combinations of pulses cannot contribute to a quadrilinear signal.
14. We set $\hbar = 1$.
15. Shen, Y.-C.; Cina, J. A. *J. Chem. Phys.* **1999**, *110*, 9793.
16. The definition of the pulse propagator in Eq. (9) differs from that used in Reference 2 by a factor of $-i$. This change in definition accounts for the difference in form of Eqs. (7) and (8) from the corresponding expressions, Eqs. (9) and (10) of Reference 2.
17. See the one-dimensional interpretive diagram in Fig. 2 of Reference 2.
18. Keusters, D.; Tan, H.-S.; Warren, W. S. *J. Phys. Chem. A* **1999**, *103*, 10369.
19. The wavefunction expansion could be made in an arbitrary basis; note, however, that expanding in eigenstates of H_e - as proposed in the recent quantum holography scheme[6] - requires prior knowledge of the eigenstates of the excited-state nuclear Hamiltonian.
20. Press, W. H.; Teukolsky, S. A.; Vetterling, W. T.; Flannery, B. P. *Numerical Recipes in C: The Art of Scientific Computing*; Cambridge University Press: Cambridge, U. K., 1992.
21. Cohen-Tannoudji, C.; Diu, B.; Laloë, F. *Quantum Mechanics*; Wiley: New York, U. S. A., 1977; Vol. 1, Complement G_V.
22. We have previously discussed dynamical arguments for signal discrimination in the case of a bounded multidimensional potential energy surface. Reference 2 reasoned that evolution for long t_w on an excited-state multidimensional surface with several optically active modes will place most of the U_B and T_B wavepacket amplitude well away from the Franck-Condon point. As the T_B wavepacket undergoes additional propagation on the ground state after the t_w interval, the U_B and T_B wavepackets should not have significant overlap. For non-zero duration laser pulses, spectral discrimination also diminishes the B_0 contribution to the signal as large-amplitude multidimensional motion will disfavor the transfer of wavepacket amplitude back to the ground state after the t_w interval in the T_B operator. These arguments also extend to the U_A and T_A wavepackets.
23. Fleck, J. A., Jr.; Morris, J. R.; Feit, M. D. *Appl. Phys.* **1976**, *10*, 129.
24. For the A_0 and B_0 terms, a spatial grid from –3.5 Å to 11.5 Å with 2048 equally spaced grid points was used. For the C_0 and D_0 terms, a spatial grid from –0.5 Å to 3.5 Å with 256 equally spaced points was used. Different spatial ranges are needed for A_0 and B_0 terms than for C_0 and D_0 terms because the wavepackets explore different spatial regions of the potentials. Different grid spacings are needed because of the differing ranges of de Broglie wavelength.
25. This choice of delay spacing avoids having a reference state that exactly matches the target state.
26. The condition number was 10^9.
27. For a recent study of target-reference overlap isolation from the nonlinear WPI signal of a model energy-transfer complex see Cina, J. A.; Kilin, D. S.; Humble, T. S. *J. Chem. Phys.* **2003**, *118*, 46.
28. Future work will examine the reconstruction of shaped wavepackets by nonlinear WPI. T. S. Humble and J. A. Cina, manuscript in preparation.